BIOCHEMISTRY
including biophysical chemistry & molecular biology
Article

Biochemistry **2009,** *48,* 5785–5793 5785
DOI: 10.1021/bi802231q

Roles of Aquaporin-4 Isoforms and Amino Acids in Square Array Assembly†

Line Strand,‡ Svein Erik Moe,‡ Tom Tallak Solbu, Marianne Vaadal, and Torgeir Holen*

Department of Anatomy, Institute of Basic Medical Sciences (IMB), and Centre for Molecular Biology and Neuroscience (CMBN), University of Oslo, Oslo, Norway ‡These authors contributed equally to this study.

Received December 6, 2008; Revised Manuscript Received May 15, 2009

ABSTRACT: Aquaporin-4 (AQP4) is a water channel found at high concentrations around blood vessels in the brain and is organized into elaborate assemblies called square arrays. The natural functions of AQP4 and the square arrays remain unknown, but under pathophysiological conditions, AQP4 has been shown to influence brain edema, synapse function, and cellular migration. AQP4 was recently found to have six isoforms, where AQP4a (also known as M1), AQP4c (also known as M23), and AQP4e are functional water transport channels. Furthermore, by two-dimensional blue native polyacrylamide gel electrophoresis (BN-PAGE) analysis of the internal composition of square arrays, three distinct isoforms were visualized. Here we combine these advances in technique with mutational analysis to test a series of current hypotheses about AQP4 functional structure. We find that the square array destabilizing N-terminus of AQP4a is partly functional through the C13 and C17 amino acids, and not through R8 and R9. We find a discrepancy between our data and the proposed tetramer−tetramer binding site based on the in vitro AQP4 two-dimensional crystal structure. On the other hand, we find that isoforms AQP4a and AQP4e, while not being able to form square arrays alone, are able to interact with AQP4c and be incorporated into higher-order structures. Our results with the novel BN-PAGE analysis technique point toward a model in which the presence of accessory isoforms (AQP4a and AQP4e) regulates the square array assembly process of the main isoform, AQP4c.

The two first isoforms of rat AQP4[1] were cloned in 1994 (*1*, *2*), but the study of square arrays by use of freeze-fracture electron microscopy goes back to the early 1970s (*3*−*5*). The linking of square arrays to aquaporins (*6*−*10*) paradoxically has obscured the function of square arrays further, since no physiological reason is known for the massive presence of water transport channels around blood vessels in the brain.

AQP4 has been linked to a long list of phenomena under pathophysiological conditions, such as brain edema, ischemic stroke, synapse function, and cellular migration (*11*−*13*). Recently, a link was found to the autoimmune demyelinating disease neuromyelitis optica (NMO), a severe inflammatory, multiple sclerosis-like disorder, which predominantly affects the optic nerve and spinal cord, as anti-AQP4 antibodies were identified in NMO patients (*14*).

Rash and co-workers demonstrated a difference in the two classical isoforms, AQP4a and AQP4c [also known as (aka) M1 and M23, respectively], with only AQP4c able to reconstitute square array-like assemblies in transfected cells (*15*). This link between square array size and AQP4 isoforms is the most persuasive evidence for square array regulation, and the link has been supported by several studies (*16*−*18*).

Recently, our group demonstrated that AQP4 has at least six isoforms: AQP4a, AQP4b, AQP4c, AQP4d, AQP4e, and AQP4f. AQP4a, AQP4c, and AQP4e are functional water transport channels and AQP4b, AQP4d, and AQP4f lack exon 2 and probably do not transport water (*19*). We also developed the first biochemical assay for square arrays, using blue native PAGE (BN-PAGE) (*20*). When the internal structure of square arrays was probed using BN-PAGE, several isoforms were present in each higher-order structure (*20*). An important question facing the field is to determine the exact functions of the different AQP4 isoforms in square array assembly.

Hiroaki and co-workers recently demonstrated the crystal structure of the rat AQP4c isoform reconstituted into lipid bilayers (*17*). From the crystal structure, several questions arose, chief among them whether the crystal structure observed was identical to the regular square arrays in vivo.

Another question probed by Hiroaki et al. was the mechanism of the square array destabilizing N-terminus of AQP4a. It was proposed that the positively charged arginines (R8 and R9) blocked square array assembly by interaction with the tetramer−tetramer binding site seen in the crystal structure, in particular amino acids R108, G157, W231, I239, and Y250 (*17*).

†L.S. holds a grant from Forskerlinjen, the Medical Student Research Programme at the University of Oslo. T.T.S., S.E.M., and T.H. are funded by FUGE, the Functional Genomics programme of the Norwegian Research Council.

*To whom correspondence should be addressed: Department of Anatomy, Institute of Basic Medical Sciences (IMB), and Centre for Molecular Biology and Neuroscience (CMBN), University of Oslo, N-0317 Oslo, Norway. Telephone: +47 22 85 12 94. Fax: +47 22 85 14 93. E-mail: torgeir.holen@medisin.uio.no.

[1]Abbreviations: AQP4, aquaporin 4; BN-PAGE, blue native polyacrylamide gel electrophoresis; CK2, casein kinase II; DDM, dodecyl β-D-maltoside; FFEM, freeze-fracture electron microscopy; IMP, intramembrane particles.

Published on Web 05/15/2009

Here we test some hypotheses arising from the Hiroaki crystal structure by mutating critical amino acids and assaying the effects using BN-PAGE. We find some aspects of the Hiroaki model wanting. In particular, the proposed tetramer−tetramer binding site did not respond even to triple mutations. However, there seemed to be a clear shift to square array assembly when cysteine C13 and C17 were mutated in the N-terminus of AQP4a. Furthermore, we show that isoforms AQP4a and AQP4e, while being unable to form square arrays on their own, are able to interact with AQP4c and thus be incorporated into higher-order structures. Our results point toward a model in which the presence of accessory isoforms (AQP4a and AQP4e) regulates the assembly process of isoform AQP4c.

MATERIALS AND METHODS

Plasmid Design, Mutations and Sequencing. The series of mutated plasmids generated in this study (Figure 1A) was designed using QuikChange online software and QuikChange II XL (Stratagene).

PCR was performed using QBioTaq reagents (Q-BioGene Inc.) on a GeneAmp PCR System 9700 (Applied Biosystems). The myc-tagged plasmids were generated by PCR cloning using an AQP4 C-terminal specific primer containing the myc sequence (5′-GCGGCCG CTACAGATCCTCTTCTGAGATGA GTTTTTGTTCTCCTACAGAAG ATAATACCTCTC-3′). Primers were synthesized by Eurogentec S.A. PCR products were cloned into pCR2.1-Topo plasmids using Topo-cloning (Invitrogen) and then subcloned into the pXOOM expression plasmid (*21*). All plasmid inserts were sequenced on a 3730 DNA analyzer (Applied Biosystems).

Cell Cultures. HeLa cells were grown in Dulbecco's modified Eagle's medium (DMEM) (Invitrogen) supplemented with 1% L-glutamine (Lonza) and 10% fetal bovine serum (Gibco). Cells were plated in a 75 cm^2 flask (Corning) at a density of 20000 cells/cm^2 24 h before transfection. Cells were transfected with FuGENE 6 (Roche) according to the FuGENE Instruction Manual. Here we used 400 μL of OptiMem (Gibco) with 20 μL of FuGENE 6 (Roche) and 6.6 μg of DNA. Cells were harvested 24 h after transfection. Cells were first washed three times in phosphate-buffered saline (PBS) and then trypsinized with 1 mL of Trypsin-Versene (EDTA) (Lonza). Cells were resuspended in 9 mL of DMEM and spun at 160*g* and 4 °C for 10 min, and the supernatant was discarded. Cells were resuspended in 1 mL of PBS and moved to an Eppendorf tube before an additional spinning at 160*g* and 4 °C for 10 min. The supernatant was discarded, and samples were homogenized in a HEPES/sucrose buffer [10 mM HEPES (pH 7.4), 2 mM EDTA, 333 mM sucrose, and Complete Protease Inhibitor Cocktail (Roche)]. The homogenate was spun at 1000*g* for 10 min. The supernatant was used for subsequent BN-PAGE and SDS−PAGE analysis.

Blue Native PAGE (BN-PAGE) Analysis. BN-PAGE gels (*22*−*24*) were run essentially as described previously (*20*). Briefly, 2−10 μg of total protein from membrane fractions was mixed with 4× Native Page Sample Buffer (Invitrogen) and dodecyl β-D-maltoside (DDM, Sigma) to give a final 1% (w/v) DDM and 1× sample buffer (Figure S1 of the Supporting Information). Samples were incubated for 10 min at room temperature before a 10 min centrifugation step at 10000*g*. The supernatant was recovered and mixed with Coomassie G-250 to yield a 1:4 ratio of Coomassie G-250 to DDM. Samples were then loaded on native PAGE Novex gels (4−16%, Invitrogen). NativeMark Unstained Protein Standard (Invitrogen) was used as a molecular weight marker. Gels were run and blotted to PVDF membranes using XCell II Blot Module (Invitrogen). Briefly, the PVDF membrane was prewet for 30 s in methanol. All pads were soaked in 1× Transfer Buffer (Invitrogen) to remove air bubbles and arranged in a standard stack of pads and filter paper. The PVDF membrane was carefully rolled onto gel, and any air bubbles were removed by rolling with a glass pipet. The transfer voltage was 50 V for 1 h. Residual Coomassie G-250 was washed away with a methanol rinse step. PVDF membranes were blocked with TBST [20 mM Tris (pH 7.4), 137 mM NaCl, and 0.1% TWEEN] containing 5% dry milk powder (Fluka Analytical), and 0.05% NaN_3 (Sigma), for 60 min before overnight incubation with diluted antibodies in the same buffer.

Antibodies, Signal Detection, and Quantification. Anti-AQP4 antibodies and anti-c-myc antibodies were purchased from Santa Cruz Biotechnology (SC9888 and SC789, used at 1:10000 and 1:500 dilutions, respectively). Alkaline phosphatase-conjugated antibodies from Sigma were used as secondary antibodies and developed with ECF substrate (Amersham). Finally, blots were scanned with a Typhoon 9410 Scanner and analyzed using ImageQuant TL version 2003.02 (Amersham). Densitometric quantification of bands was performed using ImageQuant.

SDS−PAGE Analysis. SDS−PAGE analysis was performed essentially as described previously (*25*). Briefly, gels were composed of 12% Laemmli PAGE (*26*), supplemented with 3 M urea, and the loading buffer consisted of 1.7% SDS, 60 mM Tris (pH 6.8), 5% glycerol, and 100 mM DTT; 2−8 μg of protein was loaded into each well. Samples were not heated prior to being loaded (*25*). SeeBlue Plus2 Pre-Stained Standard (Invitrogen) was used as a molecular weight marker. Proteins were blotted onto PVDF membranes using Towbin buffer (25 mM Tris and 192 mM glycine) with 20% methanol and developed as for BN-PAGE gels.

RESULTS

Hiroaki and co-workers proposed that isoform AQP4a (aka M1) is unable to form square arrays because its unique 22-amino acid N-terminus has several basic amino acids (R8 and R9) interacting with, and blocking, the tetramer−tetramer binding site (*17*). We decided to test this hypothesis by mutating arginine amino acids R8 and R9 (Figure 1A) and evaluating the effect using BN-PAGE assays (*20*). We found that R8A and R9A mutations had no effect (Figure 1B). Further, we found that a double mutation, R8A/R9A, and a triple mutation, R8K/R9K/W10A, also had no effect (Figure 1B).

During this work, another paper was published by Fujiyoshi and co-workers, now proposing that it is the N-terminal cysteines (C13 and C17) that convey the blockage of square array assembly (*18*). We also tested this mechanism in our BN-PAGE assay. We found that a single C13A or C17A mutation had no effect (Figure 1C). However, with a C13A/C17A double mutation, a faint but clear change occurred (Figure 1C). Combinations of C17A and other amino acids mutations, such as S18A, R19A, and K12A, had no effect (Figure 1B and data not shown). When this key result was replicated in astrocyte cell line CRL-2006, the shift from the single mutations C13A and C17A to the double mutation C13/C17A was even more clear (Figure S3A of the Supporting Information, lane 5). Thus, we propose that the N-terminal cysteines C13 and C17 are able to influence the ability of AQP4 to aggregate into square arrays. However, because of

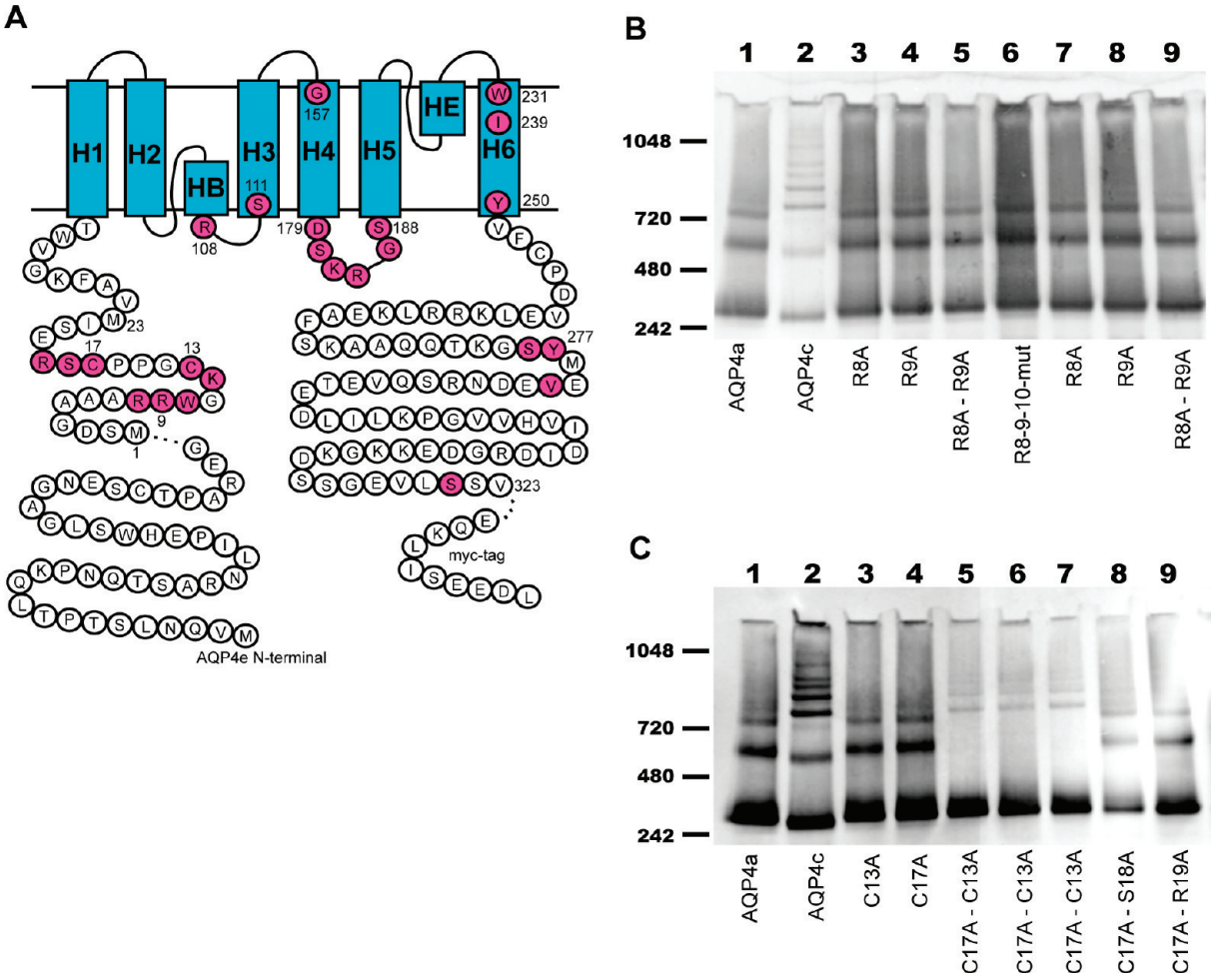

FIGURE 1: Overview of all amino acid mutations and BN-PAGE analysis of AQP4a N-terminal mutations. (A) Schematic diagram of the AQP4a transmembrane protein. Major and minor transmembrane helices are colored blue. All amino acids in the N- and C-termini are specified, and those amino acids mutated in the transmembrane region are also indicated. Numbering and red coloring indicate mutated amino acid residues. Mutations in AQP4c follow the same numbering for the sake of simplicity, resulting in the first amino acid of AQP4c being numbered amino acid 23. (B) BN-PAGE analysis of AQP4a terminal mutations. Lanes 1 and 2 were AQP4a and AQP4c controls, respectively. Single mutations were R8A (lane 3), and R9A (Lane 4). Lane 5 was the double mutation R8A/R9A and lane 6 the triple mutation R8K/R9K/W10A. Lanes 7−9 were duplicates of lanes 3−5, respectively. There were four replicate experiments. (C) BN-PAGE analysis of cysteine mutations in the N-terminus of AQP4a. Lanes 1 and 2 were AQP4a and AQP4c controls, respectively. Single mutations were C13A (lane 3) and C17A (lane 4). Double mutations were C13/C17 (lanes 5−7, in different transfection triplicates), C17/S18A (lane 8), and C17/R19 (lane 9). There were eight replicate experiments. Molecular size markers in kilodaltons are given at the left in all figures.

the incomplete shift, they are probably not the only factor. Still, the demonstrated palmitoylation of C13 and C17 (*18*) might be a regulatory mechanism for fine-tuning the structure of square arrays.

An important question arising from the Hiroaki crystal structure is whether the arrays of tetramers in the in vitro reconstituted two-dimensional (2D) crystal are identical in organization to the square arrays in vivo. A testable hypothesis is thus that the amino acids observed at the tetramer−tetramer binding sites are those responsible for tetramer−tetramer adhesion of square arrays in vivo.

We decided to test this hypothesis by mutating the amino acids proposed to constitute the tetramer−tetramer binding sites, R108, G157, W231, I239, and Y250, and thereafter assaying by BN-PAGE. We found that single mutations had no effect (Figure 2A). We reasoned that perhaps the binding strength between the tetramers was so high that a single mutation was not enough, so we proceeded to test double mutations. However, still little effect was seen (Figure 2B). Most higher-order bands on BN-PAGE gels remained stable. The only change was the 8× band (*20*), which was weakened with certain amino acids mutated (Figure 2B, lanes 4−7).

Since we did observe a weakening of the 8× band with some double mutations, we reasoned that perhaps the square arrays with the double mutations were at the critical junction before breaking down into tetramers. We decided to increase the mutation load to triple mutations. It should be noted that since the Hiroaki model includes both homomeric and heteromeric amino acid interactions, some of these triple mutations result in the breaking of up to all five bonds in the crystal structure. Still, even with loss of up to five putative interactions, with four different triple mutation constructs, the higher-order bands remained stable (Figure 2C).

Densitometric analysis of the ratio between the tetramer band and a higher-order band, in six independent gels, demonstrated no weakening of the higher-order bands relative to the tetramer band (Figure 2D). The stability of the higher-order bands of the triple mutations was replicated in astrocyte cell line CRL-2006 (Figure S3A of the Supporting Information, lanes 6−9). To control for possible loss of transport of mutated proteins to the

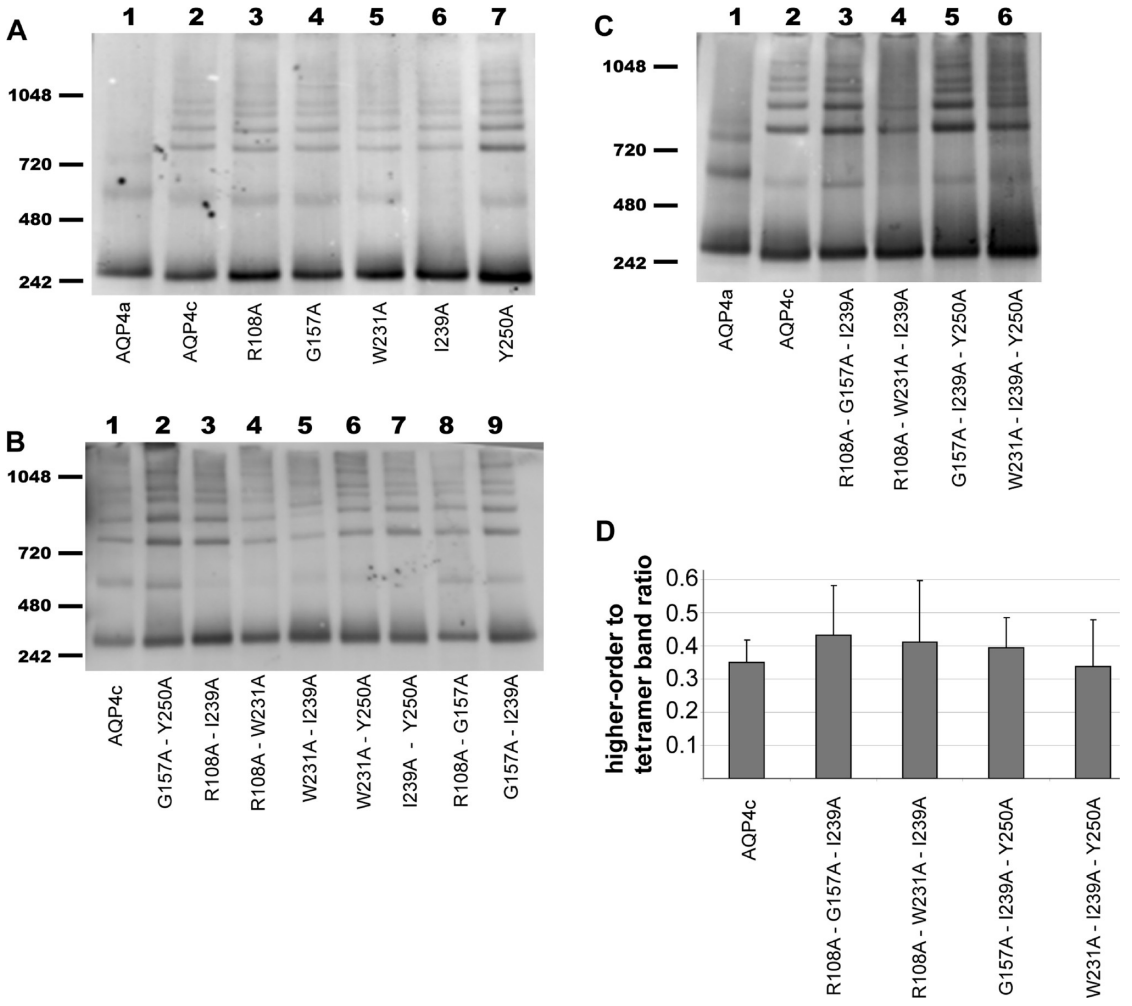

FIGURE 2: Mutational analysis of the AQP4c tetramer−tetramer binding site hypothesis by a BN-PAGE assay. (A) Single mutations in five amino acids in the proposed tetramer−tetramer interaction site. Lanes 1 and 2 were AQP4a and AQP4c controls, respectively. Single mutations R108A, G157A, W231A, I239A, and Y250A were in lanes 3−7, respectively. There were eight replicate experiments. (B) Double mutations in the proposed tetramer−tetramer binding site. Lane 1 was the AQP4c control. Lanes 2−9 were G157A/Y250A, R108A/I239A, R108A/W231A, W231A/I239A, W231A/Y250A, I239A/Y250A, R108A/G157A, and G157A/I239A, respectively. There were eight replicate experiments. (C) Triple mutations in the proposed tetramer−tetramer binding site. Lanes 1 and 2 were AQP4a and AQP4c controls, respectively. Lanes 3−6 were R108A/G157A/I239A, R108A/W231A/I239A, G157A/I239A/Y250A, and W231A/I239A/Y250A, respectively. There were six replicate experiments. Molecular size markers in kilodaltons are indicated at the left in all figures. (D) Densitometric quantification of higher-order to tetramer band, giving an average ratio for AQP4c and the triple mutations, as indicated, with the standard deviation ($n = 6$ gels analyzed).

plasma membrane, we performed an immunohistochemical study (Figure S4 of the Supporting Information). A slight tendency for more intracellular retention was seen with some mutations, but square array assembly did not seem to be affected (Figure 2C,D).

To further investigate the presence of square arrays with triple mutations, we performed BN-PAGE analysis on plasma membrane-enriched fractions [Figure S5A,B of the Supporting Information, performed essentially as described previously (*27*)]. Again the triple mutants exhibited higher-order bands (Figure S5C of the Supporting Information), although the general protein stability of the AQP4c R108A/W231A/I239A mutant protein seemed significantly lower than those of the other mutants (data not shown). Thus, the partial loss of transport to the plasma membrane seems not to be important for square array assembly, or alternatively, square array assembly can occur in intracellular vesicles.

Since higher-order bands were present with all mutations, we therefore concluded that our mutation data do not support the Hiroaki model on the proposed tetramer−tetramer interaction site for assembly of square arrays in vivo. Interestingly, however, the behavior of the 8× band, which was responsive to amino acid mutations, might suggest that the 8× complex serves in vitro as a seed for the crystallization pathway.

Phosphorylation Regulation of Square Array Assembly. If AQP4 aggregation in vivo does not follow the thermodynamically favored aggregation of reconstituted AQP4c to in vitro 2D crystals, then there is a possibility that AQP4 aggregate assembly is actively managed, thus requiring energy, which again probably necessitates regulation. The first indication that square array stability might be energy-dependent was published by Landis and Reese, indicating that square arrays were vulnerable to circulatory arrest (*28*). However, these results have not been replicated by other authorities in the field (*5*).

One possible function for square array assembly, or indeed AQP4 tetramer assembly, is concerted allosteric action, leading to closure of the water pore upon regulation. Phosphorylation is a widely used mechanism for regulation in many proteins. Several reports have been published on phosphorylation regulation of AQP4. Van Hoek and colleagues have reported that mutation of

a putative PKA phosphorylation site (S111) leads to larger square arrays and increased water permeability in LLC-PK_1 cells (*16*, *29*). Madrid et al. reported phosphorylation by casein kinase II (CK2) at sites in the C-terminus (S276, S285, and S315), regulating AQP4 internalization from the plasma membrane (*30*). Other groups have reported possible PKA phosphorylation at S111 (*31*), and PKC phosphorylation at S180 (*32*). However, a recent report found neither PKA nor PKC phosphorylation of AQP4 but did corroborate previous reports of CK2 phosphorylation of the AQP4 terminus (*33*). Interestingly, S180 is situated in loop D of AQP4, which might be involved in monomer−monomer interaction (*17*). The PDZ domain ligand at the C-terminus has also been investigated with regard to AQP4 regulation (*30*, *34*, *35*).

We tested the hypothesis of phosphorylation influence on square arrays by mutating a series of amino acids in putative phosphorylation sites, and putative loop D monomer−monomer binding sites (Figure 1A). However, in no cases, using single mutations, or using a S321-stop mutation in the PDZ domain ligand, was square array assembly affected (data not shown).

Influence of Isoform on Square Array Formation. If AQP4 aggregate assembly is not energy-dependent but still results in a well-defined, exact form, another main possibility is that the AQP4 isoforms regulate square array assembly. Rash and co-workers have shown that AQP4a and AQP4c cotransfection (M1 and M23 cotransfection) leads to a mean square array size closer to the in vivo astrocyte average of 17 IMP per square array (*15*). Our own group has recently isolated four new AQP4 isoforms (*19*) and shown that the largest isoform, AQP4e, is only weakly able to form higher-order bands on its own (*20*). Further, we demonstrated that when the internal composition of the square arrays was examined with 2D gel techniques, there seemed to be a compulsory presence of at least three isoforms (*20*).

We reasoned that it might be possible to evaluate protein−protein interactions of AQP4 isoforms using the BN-PAGE assay. Since only AQP4c is able to form very clear, distinct higher-order bands on its own (*20*), we thought cotransfection might pull other isoforms up into the higher-order bands, indicating a protein−protein interaction.

To be able to observe whether AQP4 isoforms are incorporated into the higher-order structures, the isoforms were myc-tagged at the C-terminus (Figure 1A). When the myc-tagged form of AQP4a, AQP4a-myc, was transfected into HeLa cells, only reduced amounts of higher-order structures were detected (Figure 3A, lanes 4, 6, and 8). Control transfection with AQP4c-myc showed that myc tag did not influence square array assembly (Figure 3A, lane 3). Cotransfection of AQP4a-myc and AQP4c showed that higher-order bands formed normally (Figure 3A, lanes 5, 7, and 9). When the anti-c-myc antibody was used as a probe, the myc signal was seen to be incorporated into higher-order bands (Figure 3B, lanes 5, 7, and 9). We interpret this as evidence of direct molecular interaction between AQP4c and AQP4a.

The interaction between AQP4c and AQP4a-myc was replicated in astrocyte cell line CLR-2006 (Figure S3B of the Supporting Information). To control for possible artifactual interaction between the isoforms postlysis of the cells, we performed control experiments mixing and incubating AQP4c lysates with AQP4a-myc lysates. The isoforms could not interact even at the teteramer level, as seen by the double tetramer band (Figure S2A of the Supporting Information, lane 4) and the lack

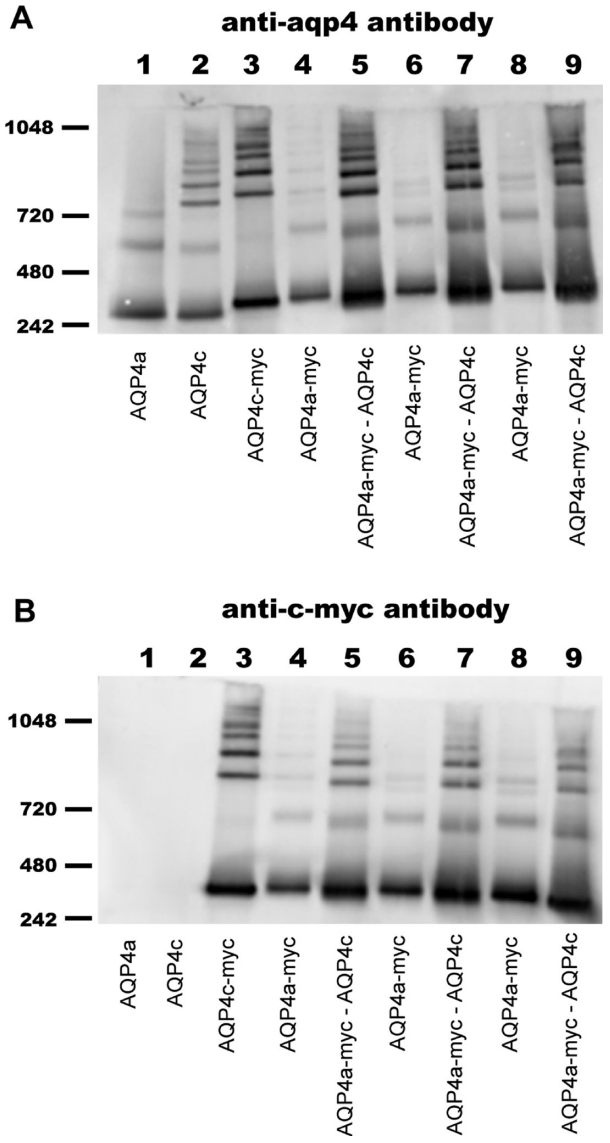

FIGURE 3: AQP4a-myc cotransfected with AQP4c in a ratio 1:1 and probing arrays with anti-aqp4 and anti-c-myc antibodies. (A) BN-PAGE analysis using the anti-AQP4 antibody. Lanes 1 and 2 were AQP4a and AQP4c controls, respectively. Lane 3 was AQP4c-myc. Lane 4 was AQP4a-myc. Lane 5 was AQP4a-myc cotransfected with AQP4c. Lanes 6 and 7, and lanes 8 and 9, were repetitions of lanes 4 and 5, respectively, with an increasing amount of cell lysate. There were 13 replicate experiments. (B) BN-PAGE analysis using the anti-c-myc antibody. Gel setup identical to that in panel A. Molecular size markers in kilodaltons are given at the left in all figures.

of myc-signal in higher-order bands (Figure S2B of the Supporting Information, lane 4).

As sensitive Western analysis of AQP4 isoform expression in rat brain shows a clear difference in the expression levels of different isoforms (*25*, *36*), we decided to test whether the relative expression levels of the AQP4a-myc and AQP4c isoforms would influence the incorporation of AQP4a-myc into higher-order bands. We first demonstrated by SDS−PAGE analysis (Figure 4A), and quantification of these gels (Figure 4B), that the expression levels of the two isoforms were a gradient from ~8:1 to ~1:5. Using anti-AQP4 antibody, square arrays were shown to form normally with cotransfections of AQP4a-myc and AQP4c, at higher AQP4c levels (Figure 4C, lanes 3−5 and 8−10).

Using BN-PAGE with the anti-c-myc antibody, we found that while the myc signals grew fainter with lower ratios of

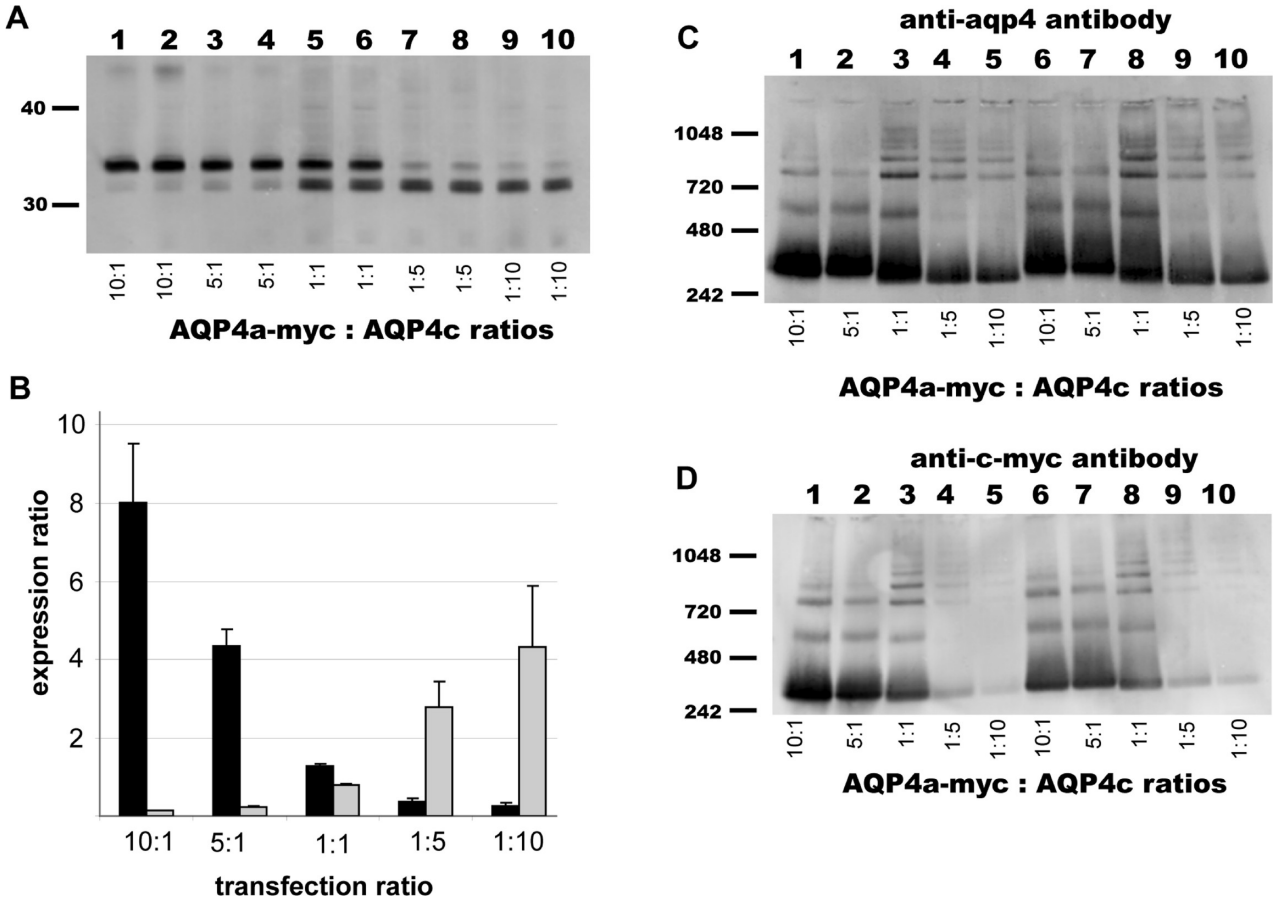

FIGURE 4: Comparisons of AQP4a square array incorporation using different expression ratios of AQP4a-myc to AQP4c. (A) SDS−PAGE analysis of 10:1 (lanes 1 and 2), 5:1 (lanes 3 and 4), 1:1 (lanes 5 and 6), 1:5 (lanes 7 and 8), and 1:10 (lanes 9 and 10) cotransfection of AQP4a-myc and AQP4c plasmids. There were four replicate experiments. (B) ImageQuant quantification of immunoblot band signal strength. Results shown are averages of six band quantifications on three different gels (black columns). The standard deviation is indicated. For the sake of clarity, inverse quantifications are also shown (gray columns). (C) BN-PAGE analysis using the anti-aqp4 antibody of a 10:1 to 1:10 AQP4a-myc:AQP4c cotransfection gradient. Lanes 1−5 were 10:1, 5:1, 1:1, 1:5, and 1:10, respectively. Lanes 6−10 were identical to lanes 1−5 with an increased amount of cell lysate. There were four replicate experiments. (D) BN-PAGE analysis using the anti-c-myc antibody of a 10:1 to 1:10 AQP4a-myc:AQP4c cotransfection gradient. Gel setup identical to that of panel C. Molecular size markers in kilodaltons are indicated at the left in all figures.

AQP4a-myc to AQP4c, the myc signal in higher-order bands was the strongest and clearest, relative to the tetramer band, at low ratios (Figure 4D). An optimal incorporation of AQP4a at lower AQP4a:AQP4c ratios is consistent with the lower expression level of AQP4a in vivo (*25*, *36*). A direct interaction between the AQP4a and AQP4c isoforms is consistent with observations by Neely and co-workers that AQP4 isolates from rat brains seem to consist of heterotetramers (*36*). Furthermore, a direct interaction is consistent with a prior study from our group analyzing the molecular composition of square array BN-PAGE bands using 2D gel technology, finding that each higher-order complex consisted of at least three isoforms (*20*).

However, a recent study by Crane and Verkman concluded that the classical AQP4-M1 (AQP4a) and AQP4-M23 (AQP4c) isoforms do not coassociate in live cells, when using quantum dot- and myc antibody-based single-molecule tracking of transfected AQP4 myc-tagged isoforms in CHO cells (*34*). Beyond speculating about whether there are some overlooked parameters in the single-molecule tracking setup or, indeed, in our own BN-PAGE setup, we cannot currently explain this discrepancy (see Discussion below).

Having established that our BN-PAGE assay could be used for protein−protein interaction studies, we proceeded to test whether the novel AQP4e isoform, tagged with myc, is incorporated into square arrays upon cotransfection. When AQP4e-myc was cotransfected with AQP4c (Figure 5A), the myc signal was seen to be incorporated into the square arrays (Figure 5B). This demonstrates a direct interaction between AQP4c and the new isoform, AQP4e. It also shows that the extra amino acids of the AQP4e N-terminus not present in AQP4a (*19*) do not block isoform−isoform interaction. Again, when expressing AQP4e-myc and AQP4c in a gradient of different ratios (Figure 6A−C), we found that AQP4e-myc was incorporated into higher-order structures at low AQP4e-myc:AQP4c ratios (Figure 6D). This seems to be consistent with the lower level of expression of the larger AQP4 isoforms in the rat brain (*25*, *36*).

DISCUSSION

Square arrays in the brain have been studied for nearly 40 years (*4*, *5*) and for the last 10−15 years have been associated with the water channel AQP4 (*7*−*10*). No natural function has been found for the extremely high densities of AQP4 around blood vessels in the brain, nor has a reason been found for the elaborate organization of a water channel into large regular arrays in the plasma membrane of astrocyte end-feet. Now progress is being made via the study of the influence of AQP4 isoforms and AQP4 amino acid composition on square array assembly.

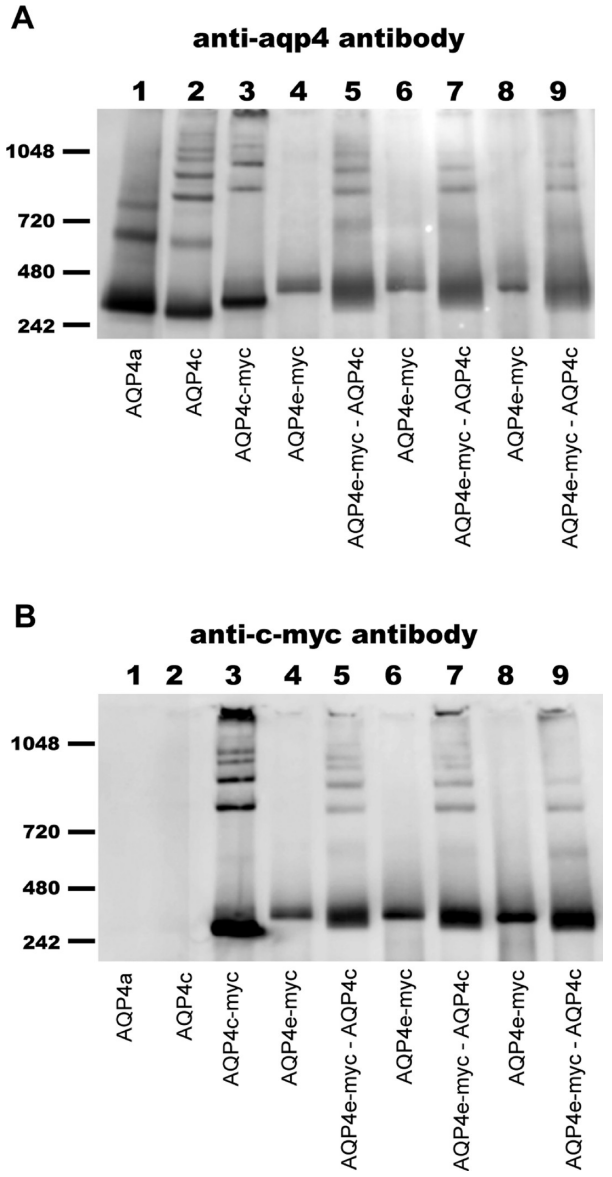

FIGURE 5: AQP4e-myc cotransfected with AQP4c in a ratio 1:1 and probing arrays with anti-aqp4 and anti-c-myc antibodies. (A) BN-PAGE analysis using anti-AQP4 antibody. Lanes 1 and 2 were AQP4a and AQP4c controls, respectively. Lane 3 was AQP4c-myc. Lane 4 was AQP4e-myc. Lane 5 was AQP4e-myc cotransfected with AQP4c. Lanes 6 and 7 and lanes 8 and 9 were repetitions of lanes 4 and 5, respectively, with increasing amounts of cell lysate. There were 12 replicate experiments. (B) BN-PAGE analysis using an anti-c-myc antibody. Gel setup identical to that for panel A. Molecular size markers in kilodaltons are indicated at the left in all figures.

Rash and co-workers quantified in a seminal paper the size distribution of thousands of square arrays in astrocyte end-feet, finding that on average a square array contains 17 intramembrane particles (IMP) (*15*). With an approximate size for the AQP4 monomer of 32−34 kDa, and assuming IMP represent a tetramer (*17*, *37*), the average square array represents a molecular complex of a total size of >2 million Da. Such a large complex must serve some function. The unknown function notwithstanding, the Gauss distribution of sizes around the mean of 17 IMP/square array indicates a precisely regulated structure size, within a spectrum of different square array sizes. A spectrum of different square arrays was also deduced in a recent study (*20*).

Experimental investigation of square arrays in cell culture using freeze-fracture electron microscopy (FFEM) was made possible by Verkman and co-workers (*8*), who demonstrated that transfection of the AQP4c isoform (aka M23, aka MIWC) into CHO cells resulted in large rafts of complexes consisting of core elements reminiscent of square arrays. Quantification by Rash and co-workers showed that such pseudosquare arrays had an average size of more than 100 IMP/square array (*15*). Quantification of cotransfection of AQP4c with the minor isoform AQP4a (aka M1) skewed the distribution toward the natural square array size of ~17 IMP.

AQP4a on its own was able to form only very small assemblies, something that a priori must be ascribed to the 22-amino acid N-terminus that AQP4c is lacking. A recent crystallization study by Fujiyoshi also found AQP4a unable to aggregate (*17*). However, the cotransfection of AQP4a and AQP4c did not reconstitute a perfect Gauss distribution around the mean of ~17 IMP/square array (*15*). Still, it was convincingly demonstrated that AQP4 isoform expression ratios could influence the size of square arrays.

Using native gel methods developed for analyzing the internal composition of square arrays, our group recently demonstrated that each higher-order complex contained at least three distinct isoforms (*20*). Further, re-examination of the AQP4 gene demonstrated the existence of at least six different isoforms, AQP4a, AQP4b, AQP4c, AQP4d, AQP4e, and AQP4f (*19*). The largest of the new AQP4 isoforms, AQP4e, like AQP4a, was unable to form square arrays on its own (*20*). These new data point toward the requirement of more than two isoforms when wild-type sized square arrays are reconstituted. In this work, we have investigated the influence of AQP4 isoforms and AQP4 amino acid residues on the square array assembly, using blue-native gels (BN-PAGE).

Fujiyoshi and co-workers proposed a mechanism based on the 2D crystal structure of AQP4 in which positively charged amino acids in the N-terminus of AQP4a blocked a tetramer−tetramer binding site (*17*). We investigated this mechanism by mutating R8 and R9 and found no change in the ability of AQP4a to form higher-order complexes (Figure 1B). On the other hand, recently a new hypothesis was proposed in a subsequent paper by Fujiyoshi and co-workers, whereby the assembly of square arrays is blocked by way of cysteines C13 and C17 in the N-terminus of AQP4a (*18*). Testing this hypothesis, we found that mutating C13 and C17 indeed led to the appearance of higher-order complexes (Figure 1C), supporting the Suzuki model and, importantly, validating our native gel analysis approach.

However, when the proposed tetramer−tetramer binding site in AQP4c was investigated (*17*), the ability of AQP4c to form square arrays was not diminished, even when all five amino acid interactions observed in the 2D crystal structure were broken (Figure 2A−C). These results would suggest that assembly of square arrays in vivo is organized differently from the reconstituted 2D crystals in vitro. Interestingly, the weakening, or loss, of the 8× band, possibly a tetramer dimer, with a higher mutational load (Figure 2B,C), might propose a solution to the crystallization path observed in vitro (*17*). A recent paper from Crane and Verkman, published during the revision of our manuscript, also supports the view that the in vitro 2D crystals are not identical to the in vivo square arrays (*38*).

That AQP4 amino acid composition does not exclusively regulate AQP4 assembly is clear from the abnormal size of transfected AQP4c pseudosquare arrays of >100 IMP, and from the shifting in the size distribution when cotransfecting with AQP4a (*15*). Having shown that BN-PAGE analysis could be

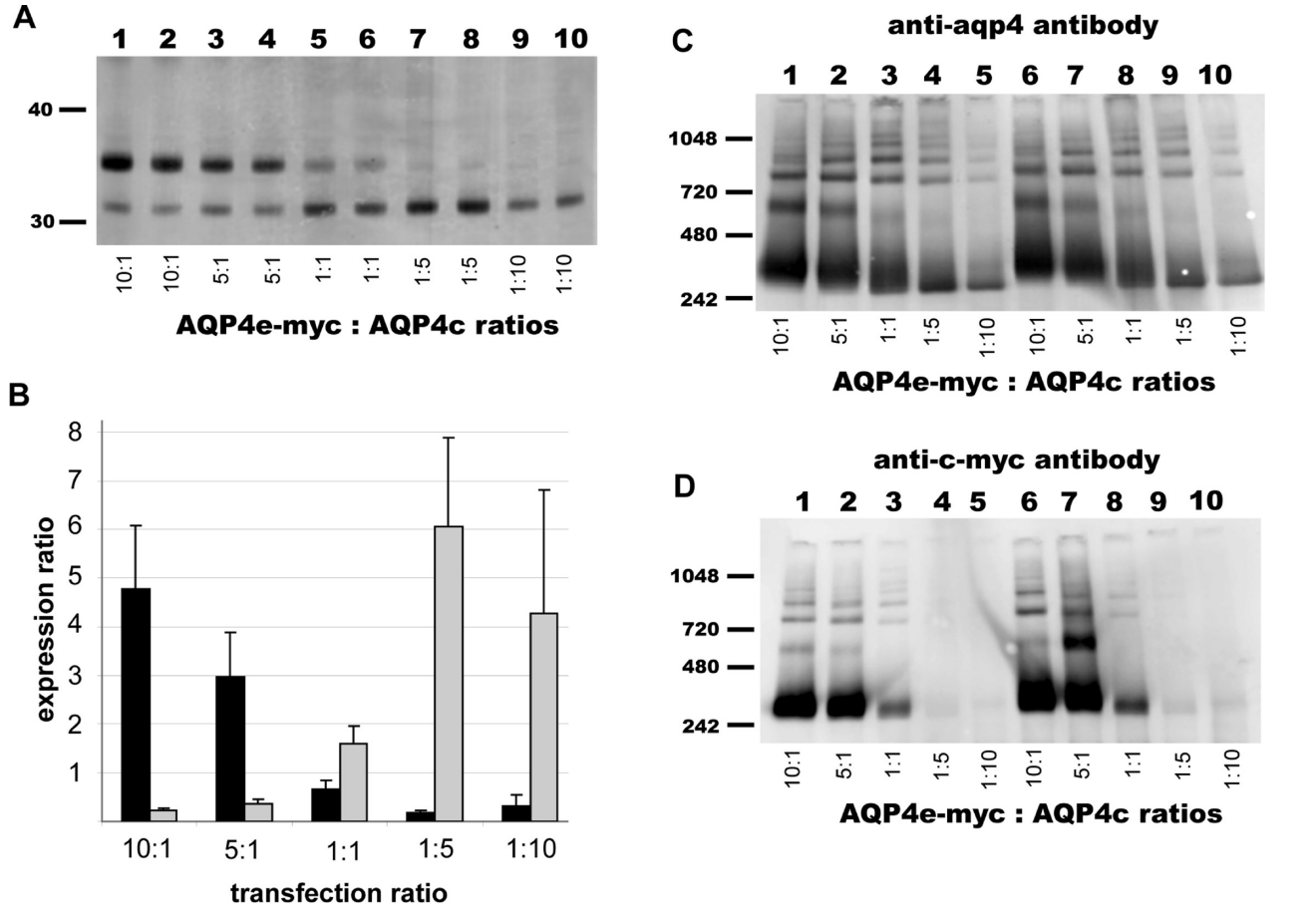

FIGURE 6: Comparisons of AQP4e square array incorporation using different expression ratios of AQP4e-myc to AQP4c. (A) SDS−PAGE analysis of 10:1 (lanes 1 and 2), 5:1 (lanes 3 and 4), 1:1 (lanes 5 and 6), 1:5 (lanes 7 and 8), and 1:10 (lanes 9 and 10) cotransfection of AQP4a-myc and AQP4c plasmids. There were three replicate experiments. (B) ImageQuant quantification of immunoblot band signal strength. Results shown are averages of four band quantifications on two different gels (black columns). The standard deviation is indicated. For the sake of clarity, inverse quantifications are also shown (gray columns). (C) BN-PAGE analysis using an anti-aqp4 antibody of a 10:1 to 1:10 AQP4e-myc:AQP4c cotransfection gradient. Lanes 1−5 were 10:1, 5:1, 1:1, 1:5, and 1:10, respectively. Lanes 6−10 were identical to lanes 1−5 with increased amounts of cell lysate. There were four replicate experiments. (D) BN-PAGE analysis using the anti-c-myc antibody of a 10:1 to 1:10 AQP4a-myc:AQP4c cotransfection gradient. Gel setup identical to that of panel C. Molecular size markers in kilodaltons are indicated at the left in all figures.

used to assay AQP4 protein−protein interactions, we went on to investigate the influence of AQP4 isoforms on square array assembly.

Using c-myc antibodies with myc-tagged AQP4 isoforms, we were able to distinguish different AQP4 isoforms in the higher-order complexes. We showed that AQP4a-myc was unable to form square arrays on its own. However, upon cotransfection with AQP4c, the myc signal was incorporated into higher-order complexes, demonstrating a molecular interaction between AQP4a and AQP4c (Figure 3B).

Crane and colleagues, using quantum dot single-molecule tracking, found no slowing of diffusion of myc-tagged AQP4a when it was cotransfected with AQP4c, thus indicating no interaction between the isoforms (*34*). We cannot explain this discrepancy at this point. However, we have briefly tested some of the AQP4c N-terminal mutations in the most recent single-molecule tracking paper (*38*), finding no complete loss of higher-order structures (Figure S6 of the Supporting Information), again indicating a discrepancy between these two assays. It is possible that diffusion interaction of AQP4a with large rafts of pseudosquare arrays does not mirror the mechanisms of the smaller complexes made visible by BN-PAGE analysis. It is also possible that the inclusion of a myc tag in loop C used for single-molecule tracking interferes with protein−protein interactions. Or, third, perhaps the dynamics of AQP4a regulation of square array size operates at shorter time scales than the single-molecule tracking time resolution. On the other hand, it has been demonstrated in previous papers that heterotetramers of AQP4a and AQP4c exist in vivo (*36*), and that higher-order complexes contain several isoforms (*20*), none of which are consistent with a lack of interaction between AQP4a and AQP4c.

The novel isoform AQP4e was also able to incorporate into square arrays (Figure 5), pointing toward a role for both AQP4a and the novel isoform AQP4e in square array assembly. Expressing different ratios of AQP4a and AQP4e to AQP4c, we found that different expression ratios influenced the efficacy of incorporation into higher-order structures. AQP4a and AQP4e were incorporated more efficiently at lower ratios of AQP4a to AQP4c (Figure 4) and AQP4e to AQP4c (Figure 6), something which is consistent with the relatively lower abundance of AQP4a and AQP4e in vivo (*25*, *36*).

The exact role of the AQP4e isoform, or indeed, of AQP4a, in the square arrays remains to be established. It is tempting, though, to speculate that while AQP4c builds the main framework, being the main building block, the AQP4a and AQP4e isoforms might serve as regulatory end points or corner blocks of the square array edifice.

SUPPORTING INFORMATION AVAILABLE

DDM detergent versus protein load calibration (Figure S1), a control for artifactual isoform−isoform interactions in the BN-PAGE setup (Figure S2), BN-PAGE analysis of AQP4 mutants and AQP4 isoform−isoform interactions in astrocyte cell line CRL-2006 (Figure S3), immunohistochemistry confocal images of AQP4 wild-type isoforms and mutants in transfected HeLa cells (Figure S4), BN-PAGE analysis of triple mutations in plasma membrane-enriched fractions (Figure S5), and BN-PAGE analysis of AQP4c N-terminal mutations (Figure S6). This material is available free of charge via the Internet at http://pubs.acs.org.

REFERENCES

(1) Hasegawa, H., Ma, T., Skach, W., Matthay, M. A., and Verkman, A. S. (1994) Molecular cloning of a mercurial-insensitive water channel expressed in selected water-transporting tissues. *J. Biol. Chem. 269*, 5497–5500.

(2) Jung, J. S., Bhat, R. V., Preston, G. M., Guggino, W. B., Baraban, J. M., and Agre, P. (1994) Molecular characterization of an aquaporin cDNA from brain: Candidate osmoreceptor and regulator of water balance. *Proc. Natl. Acad. Sci. U.S.A. 91*, 13052–13056.

(3) Dermietzel, R. (1973) Visualization by freeze-fracturing of regular structures in glial cell membranes. *Naturwissenschaften 60*, 208.

(4) Rash, J. E., Staehelin, L. A., and Ellisman, M. H. (1974) Rectangular arrays of particles on freeze-cleaved plasma membranes are not gap junctions. *Exp. Cell Res. 86*, 187–190.

(5) Wolburg, H. (1995) Orthogonal arrays of intramembranous particles: A review with special reference to astrocytes. *J. Hirnforsch. 36*, 239–258.

(6) Zampighi, G. A., Hall, J. E., Ehring, G. R., and Simon, S. A. (1989) The structural organization and protein composition of lens fiber junctions. *J. Cell Biol. 108*, 2255–2275.

(7) Frigeri, A., Gropper, M. A., Umenishi, F., Kawashima, M., Brown, D., and Verkman, A. S. (1995) Localization of MIWC and GLIP water channel homologs in neuromuscular, epithelial and glandular tissues. *J. Cell Sci. 108* (Part 9), 2993–3002.

(8) Yang, B., Brown, D., and Verkman, A. S. (1996) The mercurial insensitive water channel (AQP-4) forms orthogonal arrays in stably transfected Chinese hamster ovary cells. *J. Biol. Chem. 271*, 4577–4580.

(9) Verbavatz, J. M., Ma, T., Gobin, R., and Verkman, A. S. (1997) Absence of orthogonal arrays in kidney, brain and muscle from transgenic knockout mice lacking water channel aquaporin-4. *J. Cell Sci. 110* (Part 22), 2855–2860.

(10) Rash, J. E., Yasumura, T., Hudson, C. S., Agre, P., and Nielsen, S. (1998) Direct immunogold labeling of aquaporin-4 in square arrays of astrocyte and ependymocyte plasma membranes in rat brain and spinal cord. *Proc. Natl. Acad. Sci. U.S.A. 95*, 11981–11986.

(11) King, L. S., Kozono, D., and Agre, P. (2004) From structure to disease: The evolving tale of aquaporin biology. *Nat. Rev. Mol. Cell Biol. 5*, 687–698.

(12) Amiry-Moghaddam, M., and Ottersen, O. P. (2003) The molecular basis of water transport in the brain. *Nat. Rev. Neurosci. 4*, 991–1001.

(13) Verkman, A. S., Binder, D. K., Bloch, O., Auguste, K., and Papadopoulos, M. C. (2006) Three distinct roles of aquaporin-4 in brain function revealed by knockout mice. *Biochim. Biophys. Acta 1758*, 1085–1093.

(14) Lennon, V. A., Kryzer, T. J., Pittock, S. J., Verkman, A. S., and Hinson, S. R. (2005) IgG marker of optic-spinal multiple sclerosis binds to the aquaporin-4 water channel. *J. Exp. Med. 202*, 473–477.

(15) Furman, C. S., Gorelick-Feldman, D. A., Davidson, K. G., Yasumura, T., Neely, J. D., Agre, P., and Rash, J. E. (2003) Aquaporin-4 square array assembly: Opposing actions of M1 and M23 isoforms. *Proc. Natl. Acad. Sci. U.S.A. 100*, 13609–13614.

(16) Silberstein, C., Bouley, R., Huang, Y., Fang, P., Pastor-Soler, N., Brown, D., and Van Hoek, A. N. (2004) Membrane organization and function of M1 and M23 isoforms of aquaporin-4 in epithelial cells. *Am. J. Physiol. 287*, F501–F511.

(17) Hiroaki, Y., Tani, K., Kamegawa, A., Gyobu, N., Nishikawa, K., Suzuki, H., Walz, T., Sasaki, S., Mitsuoka, K., Kimura, K., Mizoguchi, A., and Fujiyoshi, Y. (2006) Implications of the aquaporin-4 structure on array formation and cell adhesion. *J. Mol. Biol. 355*, 628–639.

(18) Suzuki, H., Nishikawa, K., Hiroaki, Y., and Fujiyoshi, Y. (2008) Formation of aquaporin-4 arrays is inhibited by palmitoylation of N-terminal cysteine residues. *Biochim. Biophys. Acta 1778*, 1181–1189.

(19) Moe, S. E., Sorbo, J. G., Sogaard, R., Zeuthen, T., Petter, O. O., and Holen, T. (2008) New isoforms of rat Aquaporin-4. *Genomics 91*, 367–377.

(20) Sorbo, J. G., Moe, S. E., Ottersen, O. P., and Holen, T. (2008) The molecular composition of square arrays. *Biochemistry 47*, 2631–2637.

(21) Jespersen, T., Grunnet, M., Angelo, K., Klaerke, D. A., and Olesen, S. P. (2002) Dual-function vector for protein expression in both mammalian cells and *Xenopus laevis* oocytes. *BioTechniques 32* (536-8), 540.

(22) Hunte, C., von Jagow, G., and Schagger, H. (1994) Membrane Protein Purification and Crystallization: A Practical Guide , Academic Press, San Diego.

(23) Schagger, H., and von Jagow, G. (1991) Blue native electrophoresis for isolation of membrane protein complexes in enzymatically active form. *Anal. Biochem. 199*, 223–231.

(24) Wittig, I., Braun, H. P., and Schagger, H. (2006) Blue native PAGE. *Nat. Protoc. 1*, 418–428.

(25) Sorbo, J. G., Moe, S. E., and Holen, T. (2007) Early upregulation in nasal epithelium and strong expression in olfactory bulb glomeruli suggest a role for Aquaporin-4 in olfaction. *FEBS Lett. 581*, 4884–4890.

(26) Laemmli, U. K. (1970) Cleavage of structural proteins during the assembly of the head of bacteriophage T4. *Nature 227*, 680–685.

(27) Yang, B., Zhao, D., and Verkman, A. S. (2006) Evidence against functionally significant aquaporin expression in mitochondria. *J. Biol. Chem. 281*, 16202–16206.

(28) Landis, D. M., and Reese, T. S. (1981) Astrocyte membrane structure: Changes after circulatory arrest. *J. Cell Biol. 88*, 660–663.

(29) Van Hoek, A. N., Bouley, R., Lu, Y. X., Silberstein, C. M., Brown, D., Wax, M. B., and Patil, R. V. (2009) Vasopressin-induced differential stimulation of AQP4 splice variants regulates the in-membrane assembly of orthogonal arrays. *Am. J. Physiol.* (in press)

(30) Madrid, R., Le, M. S., Barrault, M. B., Janvier, K., Benichou, S., and Merot, J. (2001) Polarized trafficking and surface expression of the AQP4 water channel are coordinated by serial and regulated interactions with different clathrin-adaptor complexes. *EMBO J. 20*, 7008–7021.

(31) Carmosino, M., Procino, G., Tamma, G., Mannucci, R., Svelto, M., and Valenti, G. (2007) Trafficking and phosphorylation dynamics of AQP4 in histamine-treated human gastric cells. *Biol. Cell 99*, 25–36.

(32) Zelenina, M., Zelenin, S., Bondar, A. A., Brismar, H., and Aperia, A. (2002) Water permeability of aquaporin-4 is decreased by protein kinase C and dopamine. *Am. J. Physiol. 283*, F309–F318.

(33) Kadohira, I., Abe, Y., Nuriya, M., Sano, K., Tsuji, S., Arimitsu, T., Yoshimura, Y., and Yasui, M. (2008) Phosphorylation in the C-terminal domain of Aquaporin-4 is required for Golgi transition in primary cultured astrocytes. *Biochem. Biophys. Res. Commun. 377*, 463–468.

(34) Crane, J. M., Van Hoek, A. N., Skach, W. R., and Verkman, A. S. (2008) Aquaporin-4 dynamics in orthogonal arrays in live cells visualized by quantum dot single particle tracking. *Mol. Biol. Cell 19*, 3369–3378.

(35) Neely, J. D., Amiry-Moghaddam, M., Ottersen, O. P., Froehner, S. C., Agre, P., and Adams, M. E. (2001) Syntrophin-dependent expression and localization of Aquaporin-4 water channel protein. *Proc. Natl. Acad. Sci. U.S.A. 98*, 14108–14113.

(36) Neely, J. D., Christensen, B. M., Nielsen, S., and Agre, P. (1999) Heterotetrameric composition of aquaporin-4 water channels. *Biochemistry 38*, 11156–11163.

(37) Rash, J. E., Davidson, K. G., Yasumura, T., and Furman, C. S. (2004) Freeze-fracture and immunogold analysis of aquaporin-4 (AQP4) square arrays, with models of AQP4 lattice assembly. *Neuroscience 129*, 915–934.

(38) Crane, J. M., and Verkman, A. S. (2009) Determinants of aquaporin-4 assembly in orthogonal arrays revealed by live-cell single-molecule fluorescence imaging. *J. Cell Sci. 122*, 813–821.